Characterization of Cardiac Tissue Using High-Density Grid Catheter: Validation in Porcine Model

Lucía Ronda Rute[1], Elisa Ramírez[1], Jakub Hejč[2], Samuel Ruipérez-Campillo[3], Francisco Castells[1], Martin Pešl[2], Zdeněk Stárek[2], José Millet[1]

[1]ITACA Institute, Universitat Politècnica de València, Valencia, Spain
[2] International Clinical Research Center, St. Anne's University Hospital, Brno, Czech Republic
[3] ETH University, Zurich, Switzerland

Abstract

Accurate characterization of cardiac electrophysiological substrate is pivotal in cardiology for diagnosing and treating arrhythmias. The HD Grid catheter offers improved mapping capabilities, yet challenges persist in assessing tissue properties in data from swine undergone electroporation ablation. This study aims to characterize healthy and necrotic tissue using voltage amplitude and electrical propagation disorganization, using a Vector Field Heterogeneity (VFH) metric. We observed significant reductions in voltage amplitude and increases in heterogeneity post-ablation, indicating successful tissue modification. Correlations between voltage amplitude and heterogeneity underscore their complementary nature in tissue characterization, enhancing our understanding of cardiac tissue properties. This study categorized myocardial tissue using omnipolar amplitude and VFH, with healthy tissue showing high voltage and low heterogeneity, and necrotic tissue exhibiting low voltage and high heterogeneity, demonstrating their complementary nature in cardiac tissue characterization.

1. Introduction

Accurate characterization of the electrophysiological substrate is essential for diagnosing and treating cardiac arrhythmias [1]. The high-density HD Grid catheter (Advisor™ HD Grid mapping catheter - Abbott, St. Paul, MN, USA) has emerged as a promising tool for mapping the electrical properties of cardiac tissue (Figure 1), thanks to its 4x4 electrode configuration that reduces directional influence and improves signal acquisition [2].

Despite technological advances, challenges remain in assessing cardiac tissue properties. Traditional unipolar and bipolar signals have limitations, such as susceptibility to far-field effects and directional dependency. Omnipolar signals offer a significant improvement by mitigating these issues, leading to more precise tissue characterization [2].

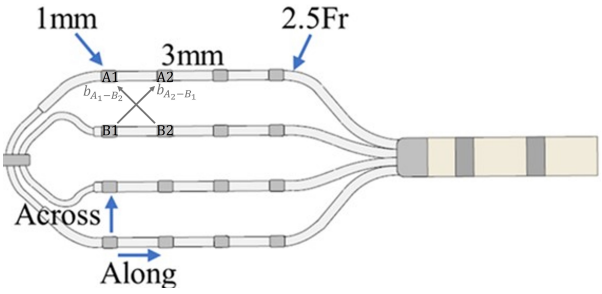

Figure 1. Advisor™ HD Grid mapping catheter - Abbott, St. Paul, MN, USA.

Omnipolar signals enable the extraction of two key parameters: Omnipolar Voltage Amplitude (OV) and Vector Field Heterogeneity (VFH). While OV overcomes the directionality dependance of bipolar amplitudes, it relies on assumptions such as tissue-electrode contact and uniform local propagation, which may not always hold true for scar tissue [2]. Myocardial thickness also affects voltage amplitude [3], necessitating the implementation of VFH to ensure study accuracy. This parameter quantifies the degree of directional propagation disorganization within cardiac tissue, offering a more comprehensive view of tissue properties [4].

Thus, this study aims to improve cardiac tissue characterization by combining OV and VFH to distinguish between healthy and necrotic tissue. By leveraging these complementary metrics, we seek to enhance the accuracy of arrhythmia diagnosis and treatment.

2. Materials

For this experiment, ECG and EGM data were collected from the left atrium of a female swine. Data were recorded using the High-Density Grid Catheter (Figure 1). Recordings were obtained at two distinct time points: previous

and immediate posterior to the ablation, which act as a reference for healthy and necrotic cardiac tissue regions. The ablation procedure was conducted using electroporation instead of traditional radiofrequency methods. This approach offers advantages such as minimal nerve and coronary damage and faster operation due to its non-thermal nature [5]. In particular, the analysis compromised 7536 unipolar EGM electrode recordings pre-ablation and 7680 recordings post-ablation.

3. Methods

All calculations detailed in this section were conducted on both pre-ablation and post-ablation datasets.

3.1. Estimation of Omnipolar EGMs

The analysis commenced with the preprocessing of unipolar electrograms (uEGM) recordings. We obtained the bipolar electrograms (bEGM) b_x and b_y in a cross formation. For instance, for the initial clique, the bipoles were generated as b_{A1-B2} and b_{A2-B1} (Figure 1) before being rotated a 45°. This arrangement offers reduced sensitivity to wavefront directionality and minimizes misalignments in comparison with other classical arrangements as the triangular one [6]. Following the computation of cross bipolar electrogram (bEGM), we conducted signal preprocessing to remove baseline wander using a median filter.

Given that the electrode is positioned within the atrium, the detection of activity in the ventricles is regarded as interference originating from a far-field source. To mitigate this , the *activation window* in bipolar electrograms (bEGMs) was selected based on the P-wave interval observed in the electrocardiogram (ECG).

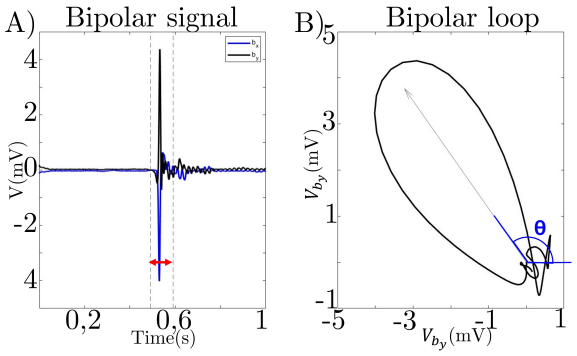

Figure 2. A) Bipoles b_x and b_y represented over time, with the vertical lines indicating the activation window. B) Graphical representation of the bipoles b_x in the x-axis and b_y in the y-axis. The arrow indicates the propagation direction and θ the propagation angle.

To calculate the Omnipolar Electrogram (oEGM), we rotate the bipoles by an angle equal to the propagation angle θ, as shown in Figure 2.

$$\begin{bmatrix}\text{omnipole}\\ \text{residue}\end{bmatrix} = \begin{bmatrix}\cos(\theta) & -\sin(\theta)\\ \sin(\theta) & \cos(\theta)\end{bmatrix} \times \begin{bmatrix}\mathrm{b}_x\\ \mathrm{b}_y\end{bmatrix} \quad (1)$$

This rotation yields two vectors: the omnipole and the residue. The omnipole represents the maximum amplitude of the activation, while the residue is the orthogonal vector describing the direction of minimum propagation.

3.2. Omnipolar parameters

3.2.1. Omnipolar amplitude

Omnipolar amplitude is the distance in voltage between the minimun and maximum points within the specified activation window in the oEGM, obtained as shown in the Equation 1. This amplitude was calculated for each clique at every catheter position.

3.2.2. Vector Field Heterogeneity

The calculation of the Vector Field Heterogeneity (VFH) metric begins with the propagation angle obtained in the subsection 3.1. From each catheter position of 4x4 electrode configuration, a 3x3 vector map is generated. This results in 9 angle values for each catheter position.

Next, from the 2D vector map, the horizontal Γ_x and vertical Γ_y components are separated:

$$(\Gamma_x)_{i,j} = \cos\theta_{i,j}; \quad (\Gamma_y)_{i,j} = \sin\theta_{i,j} \quad (2)$$

The metric computation involves forward and/or backward differences of these components in various directions within the 3x3 mesh, resulting in 4 magnitude matrices. The heterogeneity score (Ψ) is then obtained by summing the magnitudes of all 4 matrices and normalizing by the upper bound ξ, as given by the equation:

$$(\Psi)_{i,j} = \frac{\left(\frac{\Delta\Gamma}{\Delta x}\right)_{i,j} + \left(\frac{\Delta\Gamma}{\Delta y}\right)_{i,j} + \left(\frac{\Delta\Gamma}{\Delta d_1}\right)_{i,j} + \left(\frac{\Delta\Gamma}{\Delta d_2}\right)_{i,j}}{(\xi)_{i,j}} \quad (3)$$

The average of these 9 values yields the VFH score, which ranges from 0 to 1, with 0 indicating the minimal propagation disorganization, and 1 representing the maximum disorganization. In Figure 3, there are depicted two examples of different catheter position and their respective VFH map and score.

4. Results

The bipolar peak-to-peak voltage resulted in 2.64 ± 3.10 mV pre-ablation, and 0.75 ± 1.17 mV post ablation.

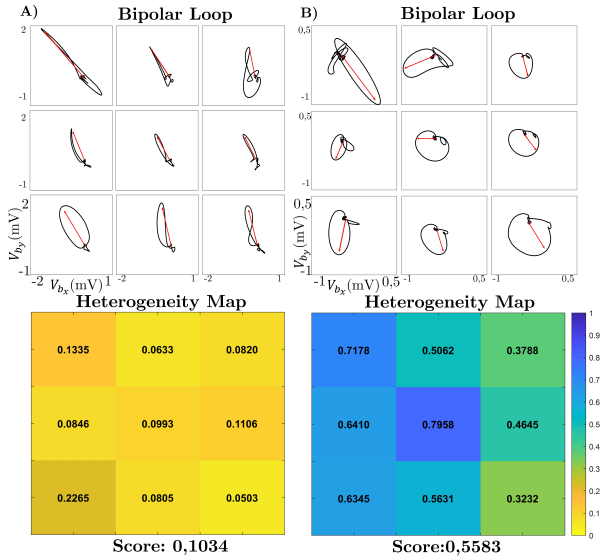

Figure 3. The bipolar vector maps and their corresponding heterogeneity map for 2 different cases, A) healthy area an B) necrotic area.

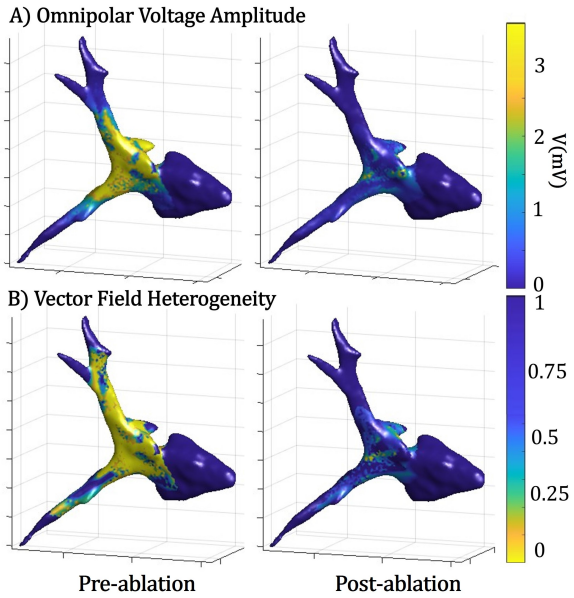

Figure 4. A) Mapping of omnipolar voltage amplitude and B) VFH scores pre and post-ablation on the left atrium of the patient.

The pre-ablation omnipolar amplitude was 2.88 ± 3.43 mV, which decreased significantly post-procedure to 0.79 ± 1.12 mV ($p < 0.001$), indicating a substantial reduction in bipolar amplitude following ablation (Figure 4 A)).

For the heterogeneity scores, there was a noticeable difference between pre-ablation ($VFH = 0.38 \pm 0.21$) and post-ablation (0.53 ± 0.13) values ($p < 0.001$) (Figure 4 B)).

The results of the VFH analysis, displayed in terms of Omnipolar Voltage (OV), revealed notable differences before and after ablation. Prior to ablation, cliques with an OV exceeding 1.5 mV exhibited a median heterogeneity score of 0.25, whereas post-ablation, this median increased to 0.36 (shown in red in Figure 5). Conversely, cliques with low OV scores under 0.5 mV (depicted in blue in Figure 5) demonstrated higher heterogeneity scores, with median values of 0.39 and 0.47 pre- and post-ablation, respectively.

5. Discussion

The effectiveness of electroporation as an ablation method is evident from the significant reduction in voltage amplitude post-ablation in both bipolar and omnipolar configurations, as observed in Figure 4 A. This reduction indicates the successful inactivation of cells in the targeted regions, where apoptosis prevents further propagation of the action potential wavefront. A key advantage of electroporation is its ability to create small, precise lesions, allowing for targeting specific areas with minimal collateral damage, thus reducing the risk of complications such as permanent nerve damage [5]. This precision allows electroporation to be potentially useful for the clinic.

By analyzing both voltage amplitude and Vector Field Heterogeneity (VFH), we can effectively characterize two distinct types of cardiac tissue. The first is healthy tissue, traditionally identified by high voltage amplitudes (Figure 4 A.), allows for effective propagation of the action potential, essential for proper heart contraction [2]. This is supported by low VFH scores (Figure 4 B.), which indicate homogeneous wavefront propagation in a consistent direction before ablation [7].

In contrast, post-ablation results characterize necrotic tissue, marked by minimal or nonexistent electrical activity (Figure 4 A.). The increased VFH scores (Figure 4 B.) in necrotic tissue reflect the disrupted propagation of the action potential due to the presence of ablation lesions, which isolate areas within the atrium and hinder uniform wavefront propagation. This disruption results in a disorganized electrical activity spread in the cavity [8].

The complementarity of VFH and voltage amplitude is particularly evident when considering their distinct advantages. While voltage amplitude can be influenced by factors like tissue thickness, which may not accurately represent cellular activity, VFH offers a more nuanced assessment of tissue properties that is independent of these factors. For instance, in areas of thinner tissue, such as around the pulmonary veins, low voltage amplitudes do not neces-

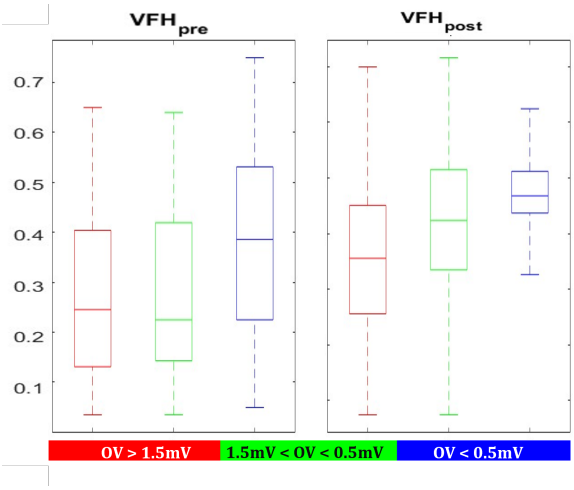

Figure 5. Heterogeneity scores distribution pre and post ablation separately, distributed in terms of Omnipolar Voltage (OV) amplitude.

sarily indicate necrosis. However, low VFH scores in these regions suggest a homogenous tissue structure, underscoring the value of combining both metrics for a comprehensive understanding of tissue characteristics. This combination enhances the ability to identify arrhythmogenic substrates and improve the targeting of ablation procedures.

6. Conclusion

This study enabled the characterization of myocardial tissue into two types: healthy and necrotic, through the combined assessment of two key parameters: omnipolar amplitude and VFH. Healthy tissue exhibits high omnipolar voltage and low heterogeneity scores, while necrotic tissue is characterized by low voltage amplitude and high heterogeneity. Thus, our findings highlight the complementary nature of these parameters in the characterization of cardiac tissue.

Acknowledgments

This work was supported by PID2022-142514OB-I00 (National Research Program, Ministerio de Ciencia e Innovación, Spanish Government) and CIBERCV CB16/11/00486 (Instituto de Salud Carlos III).

References

[1] Mavrogeni SI, Sfikakis PP, Koutsogeorgopoulou L, Markousis-Mavrogenis G, Dimitroulas T, Kolovou G, Kitas GD. Cardiac tissue Characterization and Imaging in Autoimmune Rheumatic Diseases. JACC Cardiovascular Imaging 2017;10(11):1387–1396.

[2] Deno DC, Balachandran R, Morgan D, Ahmad F, Massé S, Nanthakumar K. Orientation-Independent Catheter-Based Characterization of Myocardial Activation. IEEE transactions on biomedical engineering 2016;64(5):1067–1077.

[3] Leenknegt L, Panfilov AV, Dierckx H. Impact of Electrode Orientation, Myocardial Wall Thickness, and Myofiber Direction on Intracardiac Electrograms: Numerical Modeling and Analytical Solutions. Frontiers in Physiology 2023; 14:1213218.

[4] Pancorbo L, Ruipérez-Campillo S, Tormos Á, Guill A, Cervigón R, Alberola A, Chorro FJ, Millet J, Castells F. Vector Field Heterogeneity for the Assessment of Locally Disorganised Cardiac Electrical Propagation Wavefronts from High-density Multielectrodes. IEEE Open Journal of Engineering in Medicine and Biology 2023;.

[5] Wittkampf FH, van Es R, Neven K. Electroporation and its Relevance for Cardiac Catheter Ablation. JACC Clinical Electrophysiology 2018;4(8):977–986.

[6] Castells F, Ruipérez-Campillo S, Segarra I, Cervigón R, Casado-Arroyo R, Merino JL, Millet J. Performance Assessment of Electrode Configurations for the Estimation of Omnipolar Electrograms from High Density Arrays. Computers in biology and medicine 2023;154:106604.

[7] Sim I, Razeghi O, Solis Lemus J, Mukherjee R, O'hare D, O'neill L, Kotadia I, Roney C, Wright M, Chiribiri A, et al. Atrial Tissue Characterisation Using Electroanatomic Voltage Mapping and Cardiac Magnetic Resonance Imaging. Europace 2022;24(Supplement_1):euac053–177.

[8] Barkagan M, Leshem E, Shapira-Daniels A, Sroubek J, Buxton AE, Saffitz JE, Anter E. Histopathological Characterization of Radiofrequency Ablation in Ventricular Scar Tissue. JACC Clinical Electrophysiology 2019;5(8):920–931.

Address for correspondence:

Lucía Ronda Rute
luciaronda@outlook.es
ITACA Institute Edificio 8G, Acceso B, 1a Planta, Unversitat Politècnica de València, Camino de Vera S/N 46022 Valencia España